Exhaust particle number of a non-road diesel engine fuelled by methyl esters with different fatty acid compositions.

Agronomy Research **17**(S1), 1165–1180, 2019
https://doi.org/10.15159/AR.19.089

Exhaust particle number of a non-road diesel engine fuelled by methyl esters with different fatty acid compositions

T. Ovaska*, S. Niemi, K. Sirviö and O. Nilsson

University of Vaasa, School of Technology and Innovations, P.O. Box 700, FI-65101 Vaasa, Finland
*Correspondence: teemu.ovaska@univaasa.fi

Abstract. The main aim of this study was to find out how methyl esters with different fatty acid compositions affect the exhaust particle numbers. Along with fossil diesel fuel oil (DFO) and renewable diesel (HVO), a high-speed non-road diesel engine was fuelled by rapeseed (RME) and soybean (SME) methyl esters. Particle numbers within the size range of 5.6–560 nm were measured by means of an engine exhaust particle sizer (EEPS). The exhaust smoke, gaseous emissions and the basic engine performance were also determined. During the measurements, the 4-cylinder, turbocharged, intercooled engine was run according to the non-road steady cycle. Methyl esters reduced particles within the size range of 70 to 200 nm. For RME and SME, both positive and significant correlations were found between the sum of the particle numbers detected above the size category of 23 nm and methyl palmitate (C16:0), methyl stearate (C18:0) and methyl linoleate (C18:2) contents at 10% load at rated speed. In terms of nitrogen oxide (NO_x) and hydrocarbon (HC) emissions, HVO was beneficial while carbon monoxide (CO) emission was the lowest with DFO. The level in smoke emission was negligible.

Key words: diesel engine, particle number, methyl ester, fatty acid composition.

INTRODUCTION

The European Parliament and of the Council promoted the use of energy from renewable sources by setting the renewable energy directive in 2009. For the transport sector, the sub-target of the directive was that 10% of the fuels are from renewable sources by 2020 (Directive 2009/28/EC). In order to meet this target, the Fatty Acid Methyl Esters (FAME) has been widely used in EU as a blending component with fossil diesel fuel oil (DFO) during the past 10 years. Furthermore, the use of FAME in cultivation, transportation and distribution machineries is seen as an option for the improvement of the life cycle based greenhouse gas (GHG) balances of FAME (Jungmeier et al., 2016).

Diesel engine exhaust particles form the size distribution with two distinctive particle modes; accumulation mode and nucleation mode. The particle mean diameters in nucleation mode are under 50 nm, whereas the mean diameter range in accumulation mode is 50–500 nm (Kittelson, 1998; Rönkkö et al., 2006; Rönkkö et al., 2007; Filippo & Maricq, 2008; Lähde et al., 2010). Nucleation mode includes the particles which are believed to form during dilution when the exhaust gas gets mix up with the ambient air. Accumulation mode is thought to consist mainly of the agglomerated carbon soot

particles which result from the incomplete burning of either the fuel or the lubricating oil remnants inside the cylinder (Kittelson et al., 1999; Rönkkö et al., 2007; Nousiainen et al., 2013). Soot formation can be enhanced by improving soot oxidation (Wang et al., 2016b).

FAME fuels contain fatty acids with different lengths of molecule chains. As the molecule chain shortens, relative amount of oxygen increase in the chain. Soot oxidation improves (Pinzi et al., 2013; Barrientos et al., 2015). Moreover, the different fatty acids have divergent number of carbon–carbon double bonds in the chemical structure of FAME. Saturated fatty acids do not have double bonds while unsaturated have one or more. The less the fraction of unsaturated fatty acids the lower the soot precursors resulted from FAME fuel combustion (Zhu et al., 2016; Wang et al., 2016b).

Schönborn et al. (2009) studied the combustion behaviour of pure individual fatty acid alcohol ester molecules in a single-cylinder research engine. As a one result, particulate mass was detected to increase as the length of ester molecule was increased. They gave reason for the increased mass by means of particle numbers. Unsaturated fatty ester molecules produced more particles in the diameter range of about 40 and 200 nm compared to diesel fuel. In the study of Pinzi et al. (2013), particulate mass was increased as chain length of methyl ester was increased.

This paper presents how methyl esters with different fatty acid compositions affected the exhaust particle numbers. Along with fossil diesel fuel oil (DFO) and renewable diesel (HVO), a high-speed non-road diesel engine was fuelled by rapeseed (RME) and soybean (SME) methyl esters. Alongside the exhaust gas particle number and size distributions, the exhaust smoke, gaseous emissions and basic engine performance were determined. The high-speed off-road diesel engine was driven according to the non-road steady cycle (NRSC). During the experiments, no parameter optimization was applied with the studied fuels.

MATERIALS AND METHODS

The experimental measurements were performed by the University of Vaasa at the engine laboratory of the Technobothnia Research Centre in Vaasa, Finland.

Engine

The 4-cylinder test engine was a turbocharged, intercooled (air-to-water) off-road diesel engine, equipped with a common-rail fuel injection system. The engine had no exhaust gas after treatment. The main engine specification is given in Table 1.

Table 1. Main engine specification

Engine	AGCO POWER 44 AWI
Cylinder number	4
Bore (mm)	108
Stroke (mm)	120
Swept volume (dm^3)	4.4
Rated speed (rpm)	2,200
Rated power (kW)	101
Maximum torque with rated speed (Nm)	455*
Maximum torque with 1,500 rpm (Nm)	583*

*conformable to measured torques obtained with DFO fuel.

Fuels

The effects of rapeseed methyl ester (RME), soybean methyl ester (SME), and hydrotreated vegetable oil (HVO) on the exhaust gas particles were investigated along

with commercial low-sulphur diesel fuel oil (DFO). The fuel specifications are in Table 2. RME and SME fulfilled the requirements of EN14214 standard. DFO was used as the reference fuel, completely fulfilling the fuel standard EN590. For DFO, the lower heating value (MJ L^{-1}) was based on the information received from the fuel supplier. The unit conversion from MJ l^{-1} to MJ kg^{-1} was calculated. The lower heating values of RME, SME and HVO were computed based on the elementary analyses of fuels (Mollenhauer & Schreiner, 2010).

Table 2. Fuel specifications

Parameter	Method	DFO	RME	SME	HVO	Unit
Cetane number	ASTM D6890	-	53.5	47.3	74.7	-
Density (15 °C)	EN ISO 12185	834	883	885	779	kg m^{-3}
Sulfur content	EN ISO 20846	3.6	-	-	< 1	mg kg^{-1}
	ASTM D7039	-	< 2	3	-	mg kg^{-1}
Carbon content	ASTM D5291	-	77.4	77.0	84.2	wt.-%
Hydrogen content	ASTM D5291	-	12.2	11.9	15.1	w.t-%
Nitrogen content	ASTM D5291	-	< 0.2	< 0.2	-	wt.-%
Water content	EN ISO 12937	-	132	353	19	mg kg^{-1}
Kin. viscosity (40 °C)	Fuel supplier's info	-	4.5	4.1	2.9	mm^2 s^{-1}
Lower heating value	Fuel supplier's info	36.0*	-	-	-	MJ L^{-1}
	By calculating	43.2	37.7	37.2	43.8	MJ kg^{-1}

*(Teboil, 2019).

Any parameter optimization was not made with the studied fuels. The engine lubricant was the development product of the supplier. The fatty acid composition of RME and SME were analysed, Table 3.

Table 3. Fatty acid compositions for RME and SME

Methyl ester	RME %	SME %
10:0	< 0.1	-
12:0	-	0.1
14:0	< 0.1	0.1
16:0	4.5	11.2
16:1 cis	0.4	0.1
17:0	< 0.1	0.1
17:1	0.2	0.1
18:0	1.6	4.4
18:1 cis	61	21.8
18:2 konj.	-	< 0.1
18:2 n-6 cis	19.3	52.9
18:3 n-3 cis (ALA)	9.9	7.6
20:0	0.6	0.3
20:1	1.3	0.2
20:2 n-6 cis	0.1	0.1
22:0	0.3	0.3
22:1 n-9 cis	0.3	0.1
24:0	0.1	0.1
24:1	0.2	-
Saturated fatty acids total	7.1	16.7
Monounsaturated fatty acids total	63.3	22.3
Polyunsaturated fatty acids total	29.3	60.5
Iodine number	113.8	130.8

Analytical instruments

The particles from a size range of 5.6 to 560 nm were recorded by using the engine exhaust particle sizer (EEPS). The adopted measurement instruments for gaseous emissions and air mass flow rate are also listed in Table 4.

Before the measurements, the analysers were calibrated manually once a day according to the instructions of the instrument manufacturers. For the EEPS, the sample flow rate was adjusted at 5.0 L min^{-1}, and the 'SOOT' inversion was applied in the data processing (Wang et al., 2016a). The arrangement of the test bench and measurement devices is seen in Fig. 1.

Table 4. Measuring equipment for gaseous emissions and intake air

Parameter	Device	Technology
Particle number and size distribution	TSI EEPS 3090	spectrometer
Hydrocarbons	J.U.M. VE7	HFID
Smoke	AVL 415 S	optical filter
NO_x, CO, CO_2, O_2	TSI CA-6203 CA-CALC	electrochemical
NO_x, λ	WDO UniNO_x sensors	ZrO_2-based multilayer
O_2	Siemens Oxymat 61	paramagnetic
Air mass flow rate	ABB Sensyflow P	thermal mass

During the measurements, the exhaust gas sample was diluted at two stages in order to decrease the particle concentration of the sample for the EEPS. The sample was first diluted with ambient air by means of the porous tube diluter (PTD, Ntziachristos et al., 2004). Then, the sample was led through the secondary dilution, which was performed with Dekati ejector diluter. The total dilution ratio of exhaust sample was determined by simultaneously measuring CO_2 concentration before and after the dilution stages. The particle sampling system was provided by Tampere University. This study was a part of the larger measurement campaigns and emission data acquirement. In the studies of Karjalainen et al. (2014) and Alanen et al. (2017), the above-mentioned dilution devices were also used upstream of the EEPS. However, a thermodenuder was not employed in this study (An et al., 2007).

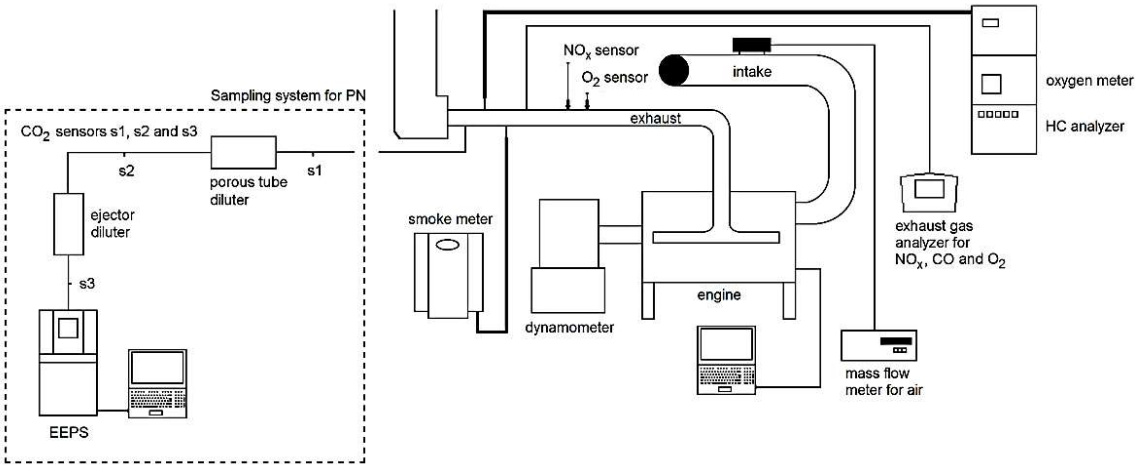

Figure 1. Experimental set-up.

The particle number (PN) was recorded consecutively three times. Each recording was one-minute long. The averaging interval of 2 seconds was used when the data was stored. The uncertainty of the PN measurement was approximated by calculating the standard deviation of the PN averages, taken from each one-minute recording.

Total particle numbers (TPN, from 5.6 to 560 nm) were calculated from the PN recordings by adding up the PN concentrations indicated in the size bins of the EEPS spectrometer during the one averaging interval. For the presented results of this paper, the average of PN sums was calculated. Moreover, the averages of the normalized PN concentrations ($dN/d\log D_p$) were calculated from each bin in order to illustrate the particle size distributions.

Based on the measured CO_2 concentrations before and after the dilution stages, the dilution ratios were calculated both for the porous type diluter (DR_{PTD}) as in (1) and for the ejector diluter ($DR_{ejector}$) as in (2). Then, the total dilution ratio (DR_{tot}) was calculated as in (3).

$$DR_{PTD} = \frac{(CO_2)_{s1} - (CO_2)_{bg}}{(CO_2)_{s2} - (CO_2)_{bg}} \quad (1)$$

$(CO_2)_{s1}$ and $(CO_2)_{s2}$ are the CO_2 concentrations of raw exhaust and diluted exhaust after first dilution stage, respectively. $(CO_2)_{bg}$ is the ambient CO_2 concentration.

$$DR_{ejector} = \frac{(CO_2)_{s2} - (CO_2)_{bg}}{(CO_2)_{s3} - (CO_2)_{bg}} \quad (2)$$

$(CO_2)_{s3}$ is the CO_2 concentration after the dilution stages before the EEPS.

$$DR_{tot} = DR_{PTD} \cdot DR_{ejector} \quad (3)$$

The calculated TPN averages and the averages of the normalized PN concentrations were multiplied by the DR_{tot} of the exhaust sample in order to present the corresponding concentrations in the raw exhaust.

However, no consistent conclusions could be drawn concerning the particle numbers under the size category of 20 nm due to the following reasons. Firstly, mobility particle size spectrometers, as EEPS, have been found to be best for the measurement of the particle numbers within the size range of 20–200 nm (Wiedensohler et al., 2012). Outside this size range, the elevated uncertainties may exist as described by Wiedensohler et al. (2018). Secondly, the nucleation mode formation has been reported to be sensitive not only to the engine parameters (Lähde et al., 2011), fuel and lubricating oil characteristics (Vaaraslahti et al., 2005), and exhaust after-treatment (Maricq et al., 2002), but also to dilution conditions such as dilution ratio, temperature and relative humidity of the dilution air (Mathis et al., 2004). On the other hand, Rönkkö et al. (2007) reported that its formation was insensitive to the fuel sulphur content, dilution air temperature, and relative humidity of ambient air.

The recorded particle numbers below 23 nm were omitted due to the two reasons. The first reason was the uncertainties related to the complex nature of nucleation mode PN and the PN measurement by means of EEPS under the size category of 20 nm. The second reason was the PN legislation which limits the particle number from the size of 23 nm on. Thus, the calculated TPN was divided into two categories depending on how many of the particles out of the average TPN were below or above the size category of 23 nm.

The authors of this paper believe the nucleation mode formation could be avoided if a thermodenuder is employed during the PN measurement (An et al., 2007). According to Vaaraslahti et al. (2004), the nucleation mode evaporates completely when an exhaust sample is heated enough.

The recorded smoke value was the average of three consecutively measured smoke numbers.

The sensor data were collected and the engine control parameters were followed via engine management software, provided by the engine manufacturer. By using the software, the temperatures of cooling water, intake air and exhaust gas plus the pressures of the intake air and exhaust gas were recorded.

Based on the measured hydrocarbon (HC), nitrogen oxides (NO_x) and carbon monoxide (CO) concentrations, the brake specific emissions of HC, NO_x and CO were calculated according to the ISO 8178 standard.

Experimental matrix and running procedure

The measurements were conducted according to the test cycle C1 of the ISO 8178-4 standard, known as the non-road steady cycle (NRSC) (ISO 8178-4:2017, 2017). The rated speed of the engine was 2,200 rpm and the intermediate speed was chosen to be 1,500 rpm. At full load, the maximum torque was 410 nm at rated speed and 525 nm at intermediate speed. The test engine was installed in a test bed and loaded by means of an eddy-current dynamometer of model Horiba WT300.

Each day before the measurements, the intake air temperature was adjusted at 50 °C downstream the charge air cooler when the engine was run at full load at rated speed. The temperature was controlled manually by regulating cooling water flow to the heat exchanger. After this initial adjustment, the temperature was allowed to change with engine load and speed. The engine was then run according to the NRSC cycle for the measurements.

Before the recordings at each load point, it was waited that the engine had stabilized, the criteria being that the temperatures of coolant water, intake air and exhaust were stable. The length of the measurement period was not tied to a certain time apart from the particle mass collection.

All measurement values were recorded once at each load point of the cycle. The particle number and size distribution were recorded continuously at each load point. For each fuel, the engine warm up and measurements were performed in an exactly similar way.

The original target was to keep the engine injection parameters constant for all fuels. Due to the lower heating values, the injection rate had, however, to be raised at full loads when the engine was run with the methyl esters. Pre-, main, and post-injections were used for the fuel injection. The upper limits of the total injection rates were changed in the electronic control unit of the engine by means of the WinEEM4 program.

The control system enabled the shift of injection quantity within the entire full load (ultimate torque) curve, Fig. 2. For RME and SME, the required increases in the injection rates were from 95 mg to 100 mg at 1,400 rpm and at 1,500 rpm. With these increases, a proper shape of the injection rate curve could be maintained. For all fuels, the position of the limited injection was also moved from 2,200 rpm to 2,250 rpm.

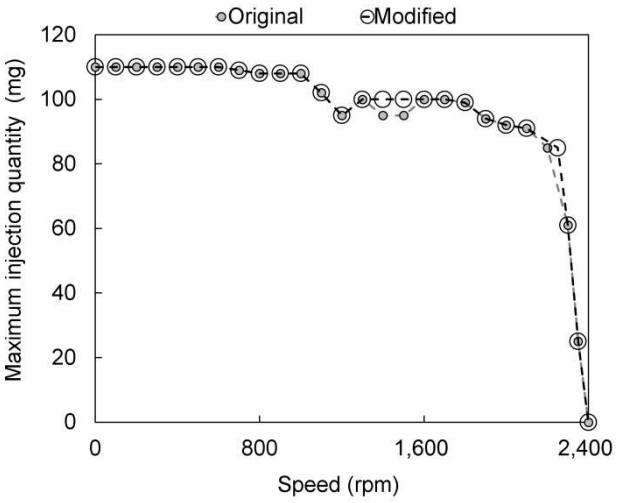

Figure 2. Upper limits of total injection rates at engine operation area.

Fig. 3, a and 3, b show the shares of the pre-, main, and post-injection rates at the load points of the NRSC cycle. For the methyl

esters, the main injection rates were higher than for DFO or HVO since the lower heating value of the esters were lower than those of DFO and HVO.

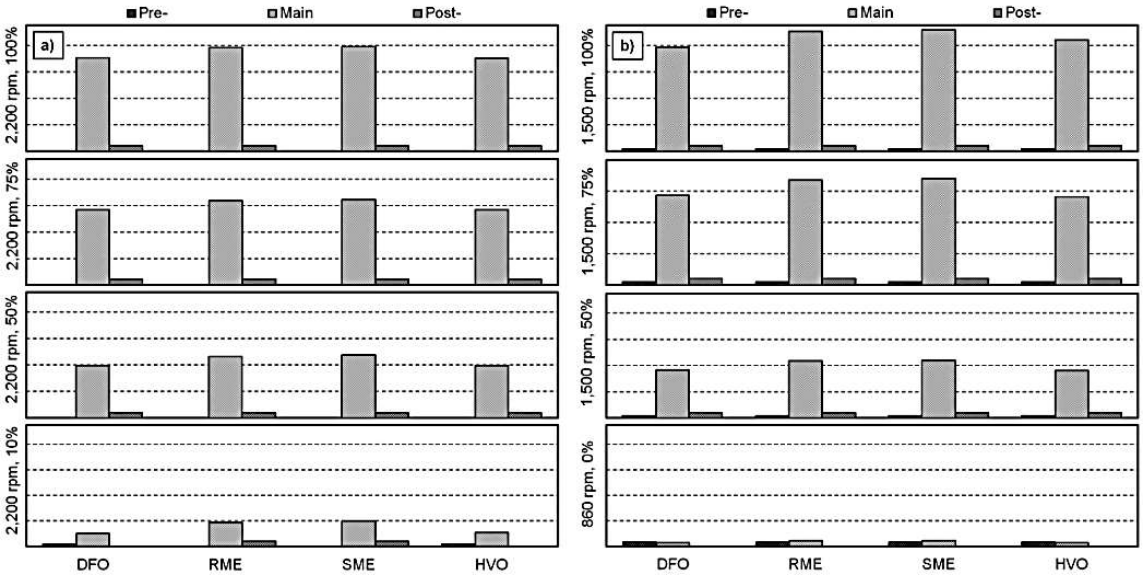

Figure 3. The shares of the pre-, main, and post-injection rates a) at 2,200 rpm and b) at 1,500 rpm and at idle.

RESULTS AND DISCUSSION

Particle size distributions

Due to the uncertainties related to the particle number measurement under the size category of 20 nm and the legislative limitation of PN from the size of 23 nm on, Figs. 4–6 illustrate the detected size distributions between 23 nm and 560 nm. Irrespective of fuel, the detected particles larger than 200 nm accounted for less than 1% of the particles larger than 23 nm in this study. Below, the distributions are examined more thoroughly at certain loads.

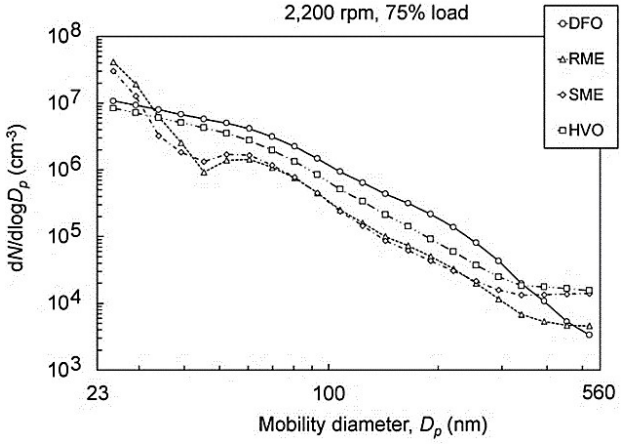

Figure 4. Exhaust particle size distributions from 23 to 560 nm at 75% load at rated speed for different fuels.

Fig. 4 shows the particle size distributions at 75% load at rated speed. Considering the particles above the size category of 23 nm, the detected distributions were quite similar for, on one hand, the methyl esters and, on the other hand, for DFO and HVO. The methyl esters produced less particles above 40 nm compared to DFO and HVO.

For 10% load, the size distributions from 23 to 560 nm are illustrated in Fig. 5. Now, the lowest PN was recorded with HVO and the highest with the methyl esters within the entire size range. The esters emitted considerably higher particle numbers than HVO and DFO.

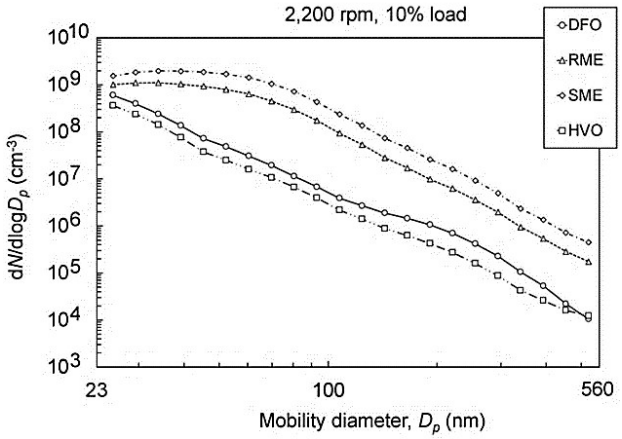

Figure 5. Exhaust particle size distributions from 23 to 560 nm at 10% load at rated speed for different fuels.

At idle (Fig. 6), HVO emitted the lowest while the methyl esters the highest PN below the size of 70 nm. The change in order of the fuels was detected above 100 nm. With the methyl esters, the lowest PN was detected from the size of 100 nm on. HVO was particularly favourable within the range of, say, below 50 nm.

The physical properties of the liquid fuel tend to control fuel spray characteristics while the fuel composition determines the pathways of chemical reactions during combustion (Eastwood, 2008). Besides the fuel sulphur content, particle formation is also influenced by other fuel characteristics such as the fuel density (Szybist et al., 2007; Bach et al., 2009), viscosity (Mathis et al., 2005; Tsolakis, 2006), cetane number (Li et al., 2014; Alrefaai et al., 2018), and the water content of fuel (Samec et al., 2002).

The current test fuels were practically free of sulphur. Therefore, the effects of sulphur could be assumed as negligible although lube oil contained sulphur. The lube oil consumption is, however, so small that the effects of sulphur compounds were assessed negligible.

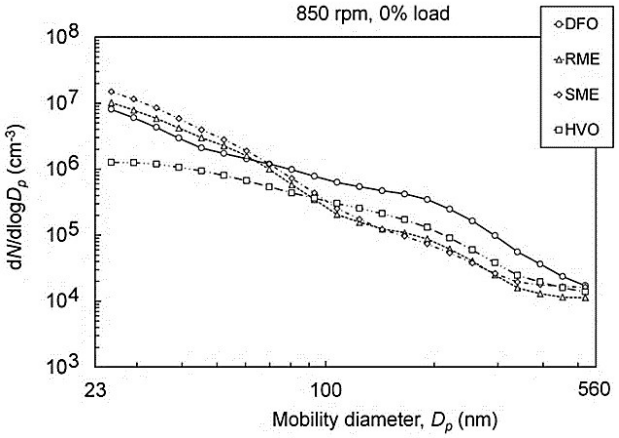

Figure 6. Exhaust particle size distributions from 23 to 560 nm at idle for different fuels.

Fuel density, viscosity, and compressibility determine the start of injection. After the injection has started, an increased cetane number leads to a shortened ignition delay plus advanced combustion. (Kegl et al., 2013). Higher fuel density and viscosity lead to an advanced start of injection. This may be followed by incomplete combustion due to poor fuel atomization. Thus, the soot emission will increase (Nabi et al., 2012).

However, the higher the water concentration in the fuel jet, the more heat is needed to vaporize the water bound by fuel. The heat absorption by water vaporization lowers the surrounding intake air temperature in the engine cylinder. As a consequence, the ignition delay period extends and thus, combustion period shortens (Samec et al., 2002;

Armas et al., 2005). This lowers the peak temperatures in combustion region due to an increase in specific heat of the air-fuel mixture around the propagating flame across the cylinder (Bedford et al., 2000). Furthermore, the vaporization of water releases oxygen which promotes soot oxidation. In this study, however, the water content of both methyl esters was low, and for DFO and HVO, negligible.

At several loads, however, the methyl esters reduced the PN within the size range of 100 to 300 nm most likely due to oxygen bounded in mono-alkyl-ester molecules (Yang et al., 2007; Lapuerta et al., 2008). More complete combustion was enabled and more effective soot oxidation was promoted during the methyl ester usage compared with DFO or HVO.

Earlier studies have also reported how FAMEs, either as neat or as blending components, had a similar decreasing effect on the number of accumulation mode particles (Jung et al., 2006; Heikkilä et al., 2009; Rounce et al., 2012). Moreover, in the study of Hellier et al. (2019), waste date pit methyl ester led to the reduced PN within the size range of 100 to 200 nm compared to fossil diesel. However, they did not detect the corresponding PN reduction with RME or SME.

Above the particle size of 23 nm at 10% load at rated speed and under 70 nm at low idle, HVO showed the most favourable PN results. This was assumed to be caused by the low sulphur content when compared to DFO, and the high cetane number when compared to the methyl esters.

Share and number of particles above 23 nm

Table 5 shows the calculated percentage shares of the particles above the size of 23 nm. At several loads, the share of the particles above 23 nm was below 10%. Irrespective of fuel, the shares greater than 10% were detected at 10% load at rated speed, and at half load at intermediate speed. Furthermore, the share of the particles above 23 nm was above 10% with HVO at full load at rated speed, with DFO at 75% load at intermediate speed, and with RME and SME at idle.

Table 5. The share of particles larger than 23 nm out of the TPN for all fuels at different loads

Speed	Rated				Intermediate			Idle
Load (%)	100	75	50	10	100	75	50	0
PN > 23 nm (%)								
DFO	4.7	5.9	5.8	20	2.5	16	52	2.8
RME	6.9	2.2	6.3	75	2.6	1.9	46	15
SME	1.5	0.9	1.4	83	1.1	0.5	45	11
HVO	16	3.0	2.8	12	1.0	2.9	48	9.4

Fig. 7 presents the sum of detected PN above 23 nm at rated speed. At full load, DFO emitted the lowest PN sum whereas HVO the highest. From 75% to 10% load, HVO emitted the lowest PN sum. The highest PN sum was then detected with either of the methyl esters.

At full load at intermediate speed, DFO emitted the lowest PN sum whereas RME the highest, Fig. 8. But at 75% load, the PN sum was the lowest with SME and the highest with DFO. The sum of detected PN above 23 nm was not varied as much at half load as at the other loads.

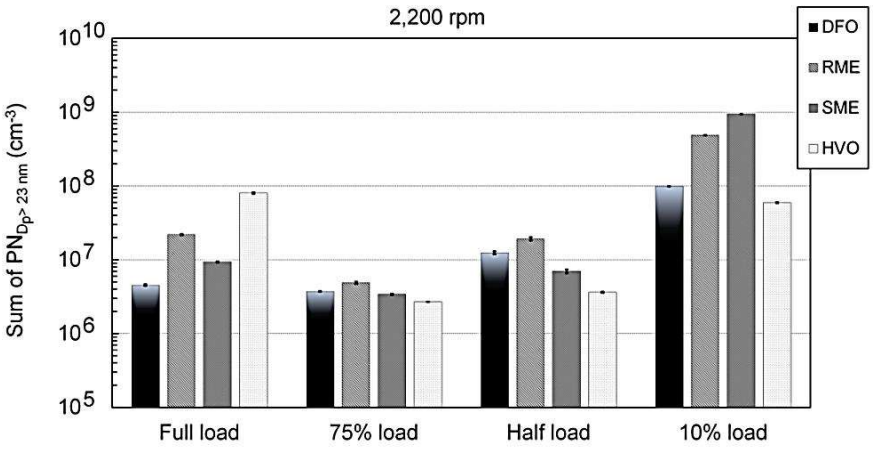

Figure 7. Sum of detected PN above 23 nm at rated speed.

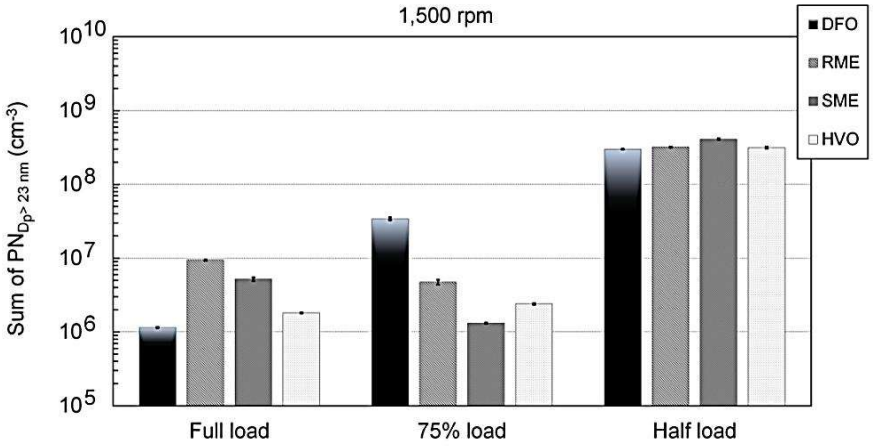

Figure 8. Sum of detected PN above 23 nm at intermediate speed.

For DFO, RME and SME, the sums of detected PN of above 23 nm were compared with the fatty acid compositions of RME and SME. DFO was selected for the comparison, as it did not contain fatty acids. Pearson correlations were calculated in order to find out measures of the strengths of relationships between the percentage shares of fatty acids and the sum of detected PN of above 23 nm. All analysed fatty acids, presented in Table 3, were considered. Moreover, the statistical significance of the correlation was assessed by using the Student's *t-test* under the null hypothesis. Significant correlations were only found between the shares of methyl palmitate (C16:0), methyl stearate (C18:0), methyl linoleate (C18:2), the saturated and the polyunsaturated fatty acids and the sum of detected PN of above 23 nm at 10% load at rated speed, Fig. 9. In this study, significant correlations did not exist at the other load points.

In general, the higher share of C16:0, C18:0, C18:2, the saturated and the polyunsaturated fatty acids, the more particles were detected above the size category of 23 nm. All correlations were both positive and significant at the confidence level of 93%. For the presented interdependences, the values of squared correlation factors were between 0.99–1.0. The calculated significance levels (*p*-values) were between

0.019–0.069. The least squares method was used to the illustrated linear fittings between the data points, Fig. 9.

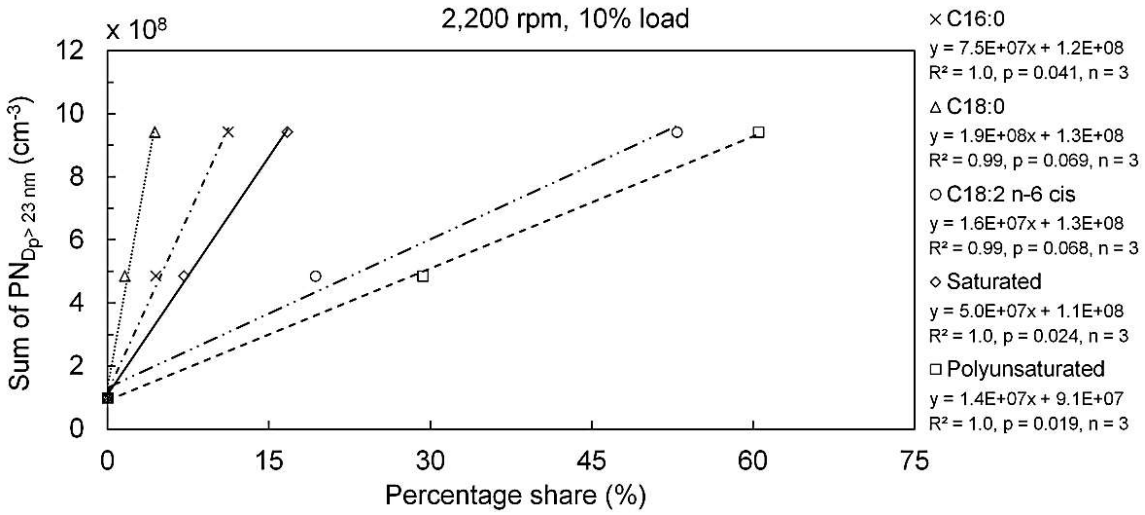

Figure 9. Sum of detected PN above 23 nm of DFO, RME and SME versus the percentage shares of C16:0, C18:0, C18:2), the saturated and the polyunsaturated fatty acids at 10% load at rated speed.

Bünger et al. (2016) found a very strong correlation between polyunsaturated fatty acids and particle mass. They fuelled a heavy-duty diesel engine with four different vegetable oils made from coconut, linseed, palm tree, and rapeseed.

Gaseous emissions and smoke

Generally, HVO was beneficial in terms of hydrocarbon (HC) and nitrogen oxide (NO_x) emissions, Table 6. Carbon monoxide (CO) emission was the lowest with DFO. The combined HC emission varied between 0.13–0.52 g kWh^{-1}. The smallest emissions, calculated all along the whole cycle, were created when HVO was used. The greatest emissions were emitted by SME.

Table 6. Cycle-weighted brake specific emissions of HC, NO_x and CO and smoke number ranges from lowest to highest within the NRSC cycle with different fuels

	HC (g kWh^{-1})	NO_x (g kWh^{-1})	CO (g kWh^{-1})	Smoke (FSN)
DFO	0.19	8.8	0.61	0.006–0.062
RME	0.38	10.0	1.55	0.005–0.012
SME	0.52	10.0	2.05	0.006–0.019
HVO	0.13	8.4	1.34	0.011–0.032

In the study of Niemi et al. (2016), the experimental setup was exactly the same when only the HC measurement is considered. For comparison, the cycle-weighted brake specific emission of HC was then 0.18 g. kWh^{-1} when DFO was used as fuel.

The less unburned HC available after fuel combustion, the smaller the likelihood that gaseous HC species affect the nanoparticle growth by condensation during the exhaust gas dilution and cooling processes (Kittelson, 1998; Khalek et al., 2000; Northrop et al., 2011).

Combined NO_x emissions varied between 8.6–10. g kWh^{-1}. The smallest NO_x emissions were created when HVO was used. The greatest NO_x emissions were emitted by RME. The difference between RME and SME was negligible. The combined CO emission varied between 0.61–2.04 g kWh^{-1}. The greatest emissions were produced by SME.

The level in smoke emission was negligible. If the test engine were a part of a typical agricultural powertrain instead of the laboratory use, it would have been equipped with an SCR catalyst. Therefore, the test engine had been tuned to the high NO_x, which caused, most likely, a decreasing effect on smoke.

Performance

The fuel conversion efficiency of the engine is presented in Figs 10 and 11 for the studied fuels at the speeds of 2,200 rpm and 1,500 rpm. The efficiencies were almost equal with the fuels.

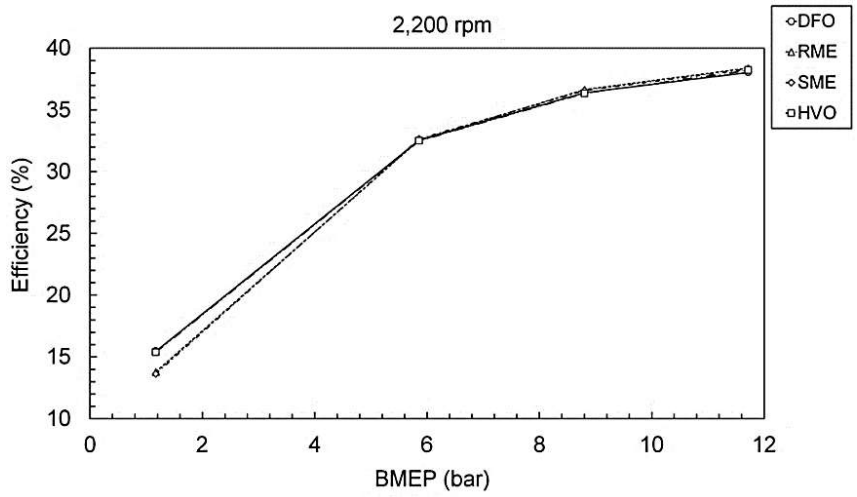

Figure 10. Engine efficiency against engine load at 2,200 rpm with the studied fuels.

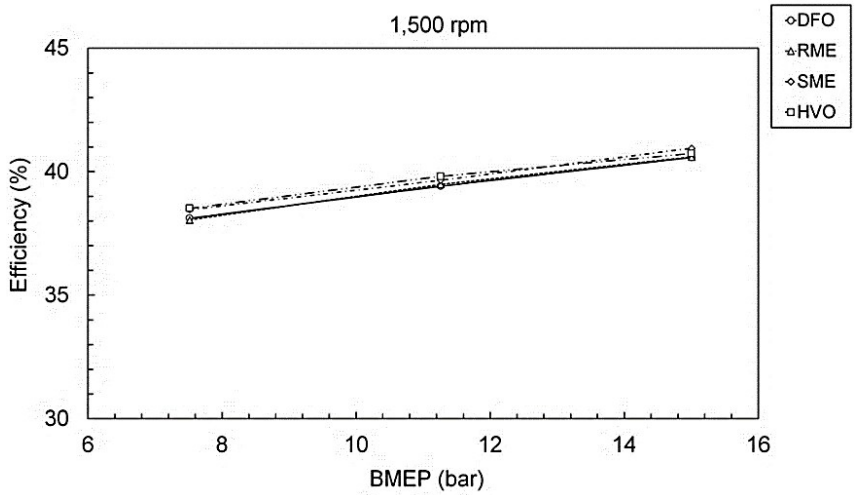

Figure 11. Engine efficiency against engine load at 1,500 rpm with the studied fuels.

CONCLUSIONS

This study focused on the determination of particle number emissions of a high-speed non-road diesel engine. The engine was driven with three bio-based fuels, RME, SME and HVO. DFO formed the baseline fuel. Based on the obtained results, the following conclusions could be drawn:

- Except at 10% load at rated speed, DFO or HVO produced the lowest particle numbers under the size of 30 nm.
- Except at 10% load at rated speed and at half load at intermediate speed, the methyl esters reduced the particle numbers within the size range of 100 to 300 nm most likely due to oxygen bounded in mono-alkyl-ester molecules.
- HVO emitted the least particles above the particle size of 23 nm at 10% load at rated speed and under 70 nm at low idle; this was assumed to be caused by the low sulphur content when compared to DFO, and the high cetane number when compared to the methyl esters.
- In case of RME and SME, both positive and significant correlations were found between the sum of the particle numbers detected above the size category of 23 nm and methyl palmitate (C16:0), methyl stearate (C18:0) and methyl linoleate (C18:2) contents at 10% load at rated speed.
- HVO was beneficial in terms of nitrogen oxide (NO_x) and hydrocarbon (HC) emissions.
- Carbon monoxide (CO) emission was the lowest with DFO.
- The level in smoke emission was negligible.

ACKNOWLEDGEMENTS. This study was one part of the national research project Trends in real-world particle emissions of diesel and gasoline vehicles (TREAM). The authors wish to thank Business Finland (former Tekes – the Finnish Funding Agency for Innovation) for the financial support of the program. AGCO Power placed the experimental engine at our disposal and the other industrial partners Dinex Ecocat Ltd, Neste, MAN and Nanol Technologies also funded the project. Our warmest thanks to all these companies. The Novia University of Applied Sciences allowed us to use the engine laboratory for this study. The authors wish to thank Dr. Jonas Waller, Mr. Holger Sved and Mr. John Dahlbacka for this possibility. The Faculty of Technology at the University of Vaasa granted the working time necessary for rendering this work into the published form. The authors wish to thank the Dean of the Faculty, Professor Erkki Antila, and Professor Timo Vekara.

REFERENCES

Alanen, J., Simonen, P., Saarikoski, S., Timonen, H., Kangasniemi, O., Saukko, E. & Keskinen, J. 2017. Comparison of primary and secondary particle formation from natural gas engine exhaust and of their volatility characteristics. *Atmos. Chem. Phys.* **17**(14), 8739–8755.

Alrefaai, M.M., Peña, G.D.G., Raj, A., Stephen, S., Anjana, T. & Dindi, A. 2018. Impact of dicyclopentadiene addition to diesel on cetane number, sooting propensity, and soot characteristics. *Fuel* **216**, 110–120.

An, W.J., Pathak, R.K., Lee, B.H. & Pandis, S.N. 2007. Aerosol volatility measurement using an improved thermodenuder: Application to secondary organic aerosol. *J. Aerosol Sci.* **38**(3), 305–314.

Armas, O., Ballesteros, R., Martos, F.J. & Agudelo, J.R. 2005. Characterization of light duty diesel engine pollutant emissions using water-emulsified fuel. *Fuel* **84**(7–8), 1011–1018.

Bach, F., Tschöke, H. & Simon, H. 2009. Influence of Alternative Fuels on Diesel Engine Aftertreatment. In: 7th International Colloquium Fuels - mineral oil based and alternative fuels 14–15th January, Ostfildern, Germany.

Barrientos, E.J., Maricq, M.M., Boehman, A.L. & Anderson, J.E. 2015. Impact of ester structures on the soot characteristics and soot oxidative reactivity of biodiesel. *SAE Tech. Pap.* 2015-01-1080.

Bedford, F., Rutland, C., Dittrich, P., Raab, A. & Wirbeleit, F. 2000. Effects of direct water injection on DI diesel engine combustion. *SAE Tech. Pap.* 2000-01-2938.

Bünger, J., Bünger, J.F., Krahl, J., Munack, A., Schröder, O., Brüning, T., Hallier, E. & Westphal, G.A. 2016. Combusting vegetable oils in diesel engines: the impact of unsaturated fatty acids on particle emissions and mutagenic effects of the exhaust. *Arch. toxicol.* **90**(6), 1471–1479.

Eastwood, P. 2008. Particulate Emissions from Vehicles. Chichester: John Wiley & Sons Ltd. 494 p. ISBN 978-0-470-72455-2.

Filippo, A.D. & Maricq, M.M. 2008. Diesel nucleation mode particles: Semivolatile or solid?. *Environ. Sci. Technol.* **42**(21), 7957–7962.

Heikkilä, J., Virtanen, A., Rönkkö, T., Keskinen, J., Aakko-Saksa, P. & Murtonen, T. 2009. Nanoparticle emissions from a heavy-duty engine running on alternative diesel fuels. *Environ. Sci. Technol.* **43**(24), 9501–9506.

Hellier, P., Jamil, F., Zaglis-Tyraskis, E., Ala'a, H., Al Haj, L. & Ladommatos, N. 2019. Combustion and emissions characteristics of date pit methyl ester in a single cylinder direct injection diesel engine. *Fuel* **243**, 162–171.

ISO 8178-4:2017. 2017. Reciprocating internal combustion engines. Exhaust emission measurement. Part 4: Steady-state and transient test cycles for different engine applications. 237 pp.

Karjalainen, P., Pirjola, L., Heikkilä, J., Lähde, T., Tzamkiozis, T., Ntziachristos, L., Keskinen, J. & Rönkkö, T. 2014. Exhaust particles of modern gasoline vehicles: A laboratory and an on-road study. *Atmos. Environ.* **97**, 262–270.

Kegl, B., Kegl, M. & Pehan, S. 2013. Green diesel engine. Biodiesel usage in diesel engines. London: Springer-Verlag. 263 p. ISBN 978-1-4471-5324-5.

Khalek, I.A., Kittelson, D.B. & Brear, F. 2000. Nanoparticle growth during dilution and cooling of diesel exhaust: Experimental investigation and theoretical assessment. *SAE Tech. Pap.* 2000-01-0515.

Kittelson, D.B. 1998. Engines and nanoparticles: a review. *J. Aerosol Sci.* **29**(5–6), 575–588.

Kittelson, D.B., Arnold, M. & Watts, W.F. 1999. Review of diesel particulate matter sampling methods: Final Report. University of Minnesota, Minneapolis, MN, 63.

Jung, H., Kittelson, D.B. & Zachariah, M.R. 2006. Characteristics of SME biodiesel-fueled diesel particle emissions and the kinetics of oxidation. *Environ. Sci. Technol.* **40**(16), 4949–4955.

Jungmeier, G., Pucker, J., Ernst, M., Haselbacher, P., Lesschen, J.P., Kraft, A., Schulzke, T. & van Loo, E.N. 2016. Improving the sustainability of fatty acid methyl esters (Fame–biodiesel)–assessment of options for industry and agriculture. In: The 24th European Biomass Conference and Exhibition, 6–9 June 2016, Amsterdam, The Netherlands.

Lapuerta, M., Armas, O. & Rodriguez-Fernandez, J. 2008. Effect of biodiesel fuels on diesel engine emissions. *Progr. Energy Combust. Sci.* **34**(2), 198–223.

Li, R., Wang, Z., Ni, P., Zhao, Y., Li, M. & Li, L. 2014. Effects of cetane number improvers on the performance of diesel engine fuelled with methanol/biodiesel blend. *Fuel* **128**, 180–187.

Lähde, T., Rönkkö, T., Happonen, M., Söderström, C., Virtanen, A., Solla, A., Kytö, M., Rothe, D. & Keskinen, J. 2011. Effect of fuel injection pressure on a heavy-duty diesel engine nonvolatile particle emission. *Environ. Sci. Technol.* **45**(6), 2504–2509.

Lähde, T., Rönkkö, T., Virtanen, A., Solla, A., Kytö, M., Söderström, C. & Keskinen, J. 2010. Dependence between nonvolatile nucleation mode particle and soot number concentrations in an EGR equipped heavy-duty diesel engine exhaust. Environ. Sci. Technol. 44(8), 3175–3180.

Maricq, M.M., Chase, R.E., Xu, N. & Laing, P.M. 2002. The effects of the catalytic converter and fuel sulfur level on motor vehicle particulate matter emissions: light duty diesel vehicles. *Environ. Sci. Technol.* **36**(2), 283–289.

Mathis, U., Mohr, M., Kaegi, R., Bertola, A. & Boulouchos, K. 2005. Influence of diesel engine combustion parameters on primary soot particle diameter. *Environ. Sci. Technol.* **39**(6), 1887–1892.

Mathis, U., Ristimaki, J., Mohr, M., Keskinen, J., Ntziachristos, L., Samaras, Z. & Mikkanen, P. 2004. Sampling conditions for the measurement of nucleation mode particles in the exhaust of a diesel vehicle. *Aerosol Sci. Technol.* **38**(12), 1149–1160.

Mollenhauer, K. & Schreiner, K. 2010. History and fundamental principles of the diesel engine. In: K. Mollenhauer & H. Tschöke (Eds.), Handbook of diesel engines, pp. 3–30. Heidelberg, Berlin: Springer-Verlag. ISBN 978-3-540-89082-9.

Nabi, M.N., Brown, R.J., Ristovski, Z. & Hustad, J.E. 2012. A comparative study of the number and mass of fine particles emitted with diesel fuel and marine gas oil (MGO). *Atmos. Environ.* **57**, 22–28.

Niemi, S., Vauhkonen, V., Mannonen, S., Ovaska, T., Nilsson, O., Sirviö, K., Heikkilä, S. & Kiijärvi, J. 2016. Effects of wood-based renewable diesel fuel blends on the performance and emissions of a non-road diesel engine. *Fuel* **186**, 1–10.

Northrop, W.F., Madathil, P.V., Bohac, S.V., Assanis, D.N. 2011. Condensational Growth of Particulate Matter from Partially Premixed Low Temperature Combustion of Biodiesel in a Compression Ignition Engine. *Aerosol Sci. Technol.* **45**, 26–36.

Nousiainen, P., Niemi, S., Rönkkö, T., Karjalainen, P., Keskinen, J., Kuuluvainen, H., Pirjola, L. & Saveljeff, H. 2013. Effect of injection parameters on exhaust gaseous and nucleation mode particle emissions of a Tier 4i nonroad diesel engine. *SAE Tech. Pap.* 2013-01-2575.

Ntziachristos, L., Giechaskiel, B., Pistikopoulos, P., Samaras, Z., Mathis, U., Mohr, M., Ristimäki, J., Keskinen, J., Mikkanen, P., Casati, R., Scheer, V. & Vogt, R. 2004. Performance evaluation of a novel sampling and measurement system for exhaust particle characterization. *SAE Tech. Pap.* 2004-01-1439.

Pinzi, S., Rounce, P., Herreros, J.M., Tsolakis, A. & Dorado, M.P. 2013. The effect of biodiesel fatty acid composition on combustion and diesel engine exhaust emissions. Fuel 104, 170–182.

Rounce, P., Tsolakis, A. & York, A.P.E. 2012. Speciation of particulate matter and hydrocarbon emissions from biodiesel combustion and its reduction by aftertreatment. Fuel **96**, 90–99.

Rönkkö, T., Virtanen, A., Vaaraslahti, K., Keskinen, J., Pirjola, L. & Lappi, M. 2006. Effect of dilution conditions and driving parameters on nucleation mode particles in diesel exhaust: Laboratory and on-road study. *Atmos. Environ.* **40**(16), 2893–2901.

Rönkkö, T., Virtanen, A., Kannosto, J., Keskinen, J., Lappi, M. & Pirjola, L. 2007. Nucleation mode particles with a nonvolatile core in the exhaust of a heavy duty diesel vehicle. *Environ. Sci. Technol.* **41**(18), 6384–6389.

Samec, N., Kegl, B. & Dibble, R.W. 2002. Numerical and experimental study of water/oil emulsified fuel combustion in a diesel engine. *Fuel* **81**(16), 2035–2044.

Schönborn, A., Ladommatos, N., Williams, J., Allan, R. & Rogerson, J. 2009. The influence of molecular structure of fatty acid monoalkyl esters on diesel combustion. *Combustion and flame* **156**(7), 1396–1412.

Teboil. 2019. Product data - summer quality. Helsinki. Available from: https://www.teboil.fi /globalassets/tuotetiedotteet/motor_lammitys-kl_2019.pdf.

Tsolakis, A. 2006. Effects on particle size distribution from the diesel engine operating on RME-biodiesel with EGR. *Energy & Fuels* **20**(4), 1418–1424.

Szybist, J.P., Song, J., Alam, M. & Boehman, A.L. 2007. Biodiesel combustion, emissions and emission control. *Fuel Process. Technol.* **88**(7), 679–691.

Vaaraslahti, K., Virtanen, A., Ristimäki, J. & Keskinen, J. 2004. Nucleation mode formation in heavy-duty diesel exhaust with and without a particulate filter. *Environ. Sci. Technol.* **38**(18), 4884–4890.

Vaaraslahti, K., Keskinen, J., Giechaskiel, B., Solla, A., Murtonen, T. & Vesala, H. 2005. Effect of lubricant on the formation of heavy-duty diesel exhaust nanoparticles. *Environ. Sci. Technol.* **39**(21), 8497–8504.

Wang, X., Grose, M.A., Caldow, R., Osmondson, B.L., Swanson, J.J., Chow, J.C., Watson, J.G., Kittelson, D.B., Li, Y., Xue, J., Jung, H. & Hu, S. 2016a. Improvement of Engine Exhaust Particle Sizer (EEPS) Size Distribution Measurement – II. Engine Exhaust Particles. *J. Aerosol Sci.* **92**, 83–94.

Wang, Z., Li, L., Wang, J. & Reitz, R.D. 2016b. Effect of biodiesel saturation on soot formation in diesel engines. *Fuel* **175**, 240–248.

Wiedensohler, A., Birmili, W., Nowak, A., Sonntag, A., Weinhold, K., Merkel, M., Wehner, B., Tuch, T., Pfeifer, S., Fiebig, M., Fjäraa, A.M., Asmi, E., Sellegri, K., Depuy, R.,Venzac, H., Villani, P., Laj, P., Aalto, P., Ogren, J.A., Swietlicki, E., Williams, P., Roldin, P., Quincey, P., Hüglin, C., Fierz-Schmidhauser, R., Gysel, M., Weingartner, E., Riccobono, F., Santos, S., Grüning, C., Faloon, K., Beddows, D., Harrison, R., Monahan, C., Jennings, S.G., O'Dowd, C.D., Marinoni, A., Horn, H.-G., Keck, L., Jiang, J., Scheckman, J., Mcmurry, P.H., Deng, Z., Zhao, C.S., Moerman, M., Henzing, B., De Leeuw, G., Löschau, G., Bastian, S. 2012. Mobility particle size spectrometers: harmonization of technical standards and data structure to facilitate high quality long-term observations of atmospheric particle number size distributions. *Atmos. Meas. Tech.* **5**, 657–685.

Wiedensohler, A., Wiesner, A., Weinhold, K., Birmili, W., Hermann, M., Merkel, M., Müller, T., Pfeifer, S., Schmidt, A., Tuch, T., Velarde, F., Quincey, P., Seeger, S. & Nowak, A. 2018. Mobility particle size spectrometers: Calibration procedures and measurement uncertainties. *Aerosol Sci. Technol.* **52**(2), 146–164.

Zhu, L., Cheung, C.S. & Huang, Z. 2016. A comparison of particulate emission for rapeseed oil methyl ester, palm oil methyl ester and soybean oil methyl ester in perspective of their fatty ester composition. *Appl. Therm. Eng.* **94**, 249–255.

Yang, H.H., Chien, S.M., Lo, M.Y., Lan, J.C. W., Lu, W.C. & Ku, Y.Y. 2007. Effects of biodiesel on emissions of regulated air pollutants and polycyclic aromatic hydrocarbons under engine durability testing. *Atmos. Environ.* **41**(34), 7232–7240.